Nuclear Instruments and Methods in Physics Research B 108 (1996) 331-338

ELSEVIER

NIM B
Beam Interactions with Materials & Atoms

The surface effect on Au 4f X-ray photoelectron spectra

J.P. Wang [a], C.J. Tung [a,*], Y.F. Chen [b], C.M. Kwei [c]

[a] Department of Nuclear Science, National Tsing Hua University, Hsinchu, Taiwan, ROC
[b] Precision Instrument Development Center, Science-Based Industrial Park, Hsinchu, Taiwan, ROC
[c] Department of Electronics Engineering, National Chiao Tung University, Hsinchu, Taiwan, ROC

Received 2 June 1995; revised form received 22 August 1995

Abstract

An investigation of the surface effect on Au 4f X-ray photoelectron spectra was made for different emission angles. It was found that surface plasmon excitations made significant contributions to the spectra in single and plural energy-loss peaks and in the multiple loss background. Our approach involved Monte Carlo simulations of photoelectrons in the interior region of the solid and Poisson stochastic processes in the surface region. The partial-wave expansion method with the Hartree–Fock–Wigner–Seitz potential for the solid was used to calculate differential electron elastic scattering cross sections. An extended Drude dielectric function model was employed to compute electron differential inverse mean free paths for volume excitations. The inelastic mean free paths in the surface region became spatially-varying and were calculated. Differential probabilities for surface excitations were determined using the same model dielectric function. The computed X-ray photoelectron spectra including surface excitations agreed quite well with experimental data.

1. Introduction

A quantitative description of the angular distribution and energy spectra of electrons emitted by a solid sample is important in surface analyses. X-ray photoelectron spectroscopy (XPS), for instance, is a powerful technique applied in surface compositional analysis [1], i.e. electron spectroscopy for chemical analysis (ESCA). Theoretical XPS studies require information on both elastic and inelastic interactions for electrons with energies below, say, 2000 eV [2] in solids. For inelastic interactions, it is the excitations of the valence band that dominate the energy losses of the detected electrons. Both volume (including bulk plasmons and interband transitions) and surface (surface plasmons) excitations contribute to the XPS. Single and plural excitations give rise to prominent loss peaks, whereas multiple excitations lead to the peak background.

Monte Carlo (MC) simulations are widely applied in quantitative surface analyses. Analyses for XPS have either ignored elastic electron scattering [3–5] or considered both elastic scattering and inelastic volume excitations [6–9]. The contribution from surface excitations was never considered until recent work [10] showed an effective loss-function extracted from measured Au 4f XPS data at 45° exit angle. This function, however, was later found to yield incorrect spectra at other exit angles [11]. It was then argued that the effective loss-function was dependent on the exit angle. Previously, we have successfully incorporated surface excitations into models for reflection electron-energy-loss spectroscopy (REELS) [12,13]. Our work made use of an energy-loss function established by the dielectric response theory. Differential cross sections for inelastic interactions were constructed separately for surface and volume excitations. The calculated REELS was compared with experimental data [14] and other theoretical results [15]. Thus, it seems plausible to derive XPS using detailed cross sections calculated from first principles.

In this work, we investigate the surface effect on Au 4f XPS for different exit angles. Our approach involves MC simulations of photoelectrons in the interior of the solid, referred to as the deep region, and Poisson stochastic processes near the surface, i.e. the shallow region. The Poisson process is valid since the shallow region extends into the solid only a few angstroms, on the order of one inelastic mean free path (MFP). Thus, electron inelastic MFP in the shallow region may be assumed to be a constant everywhere inside this region. In addition, this process makes use of the total probability for inelastic interactions rather than the differential probability per unit pathlength required by MC simulations. Since the latter quantity becomes spatially-varying in the shallow region [16], it is very difficult to apply it in MC simulations. In this work, we use the partial-wave expansion method with the Hartree–Fock–Wigner–Seitz (HFWS) potential for a solid to calculate electron differential elastic cross sections [13]. An extended Drude dielectric function model [17] is

* Corresponding author. Tel. +886 35 727300, fax +886 35 718649, e-mail cjtung@ins.nthu.edu.tw.

SSDI 0168-583X(95)01058-0

employed to compute electron differential inverse mean free paths (DIMFP) for volume excitations. The spatially-varying DIMFPs in the shallow region are also established. Differential probabilities for surface excitations are determined using the same model dielectric function. All cross section data are then substituted into a program to compute Au 4f XPS with and without the contributions from surface excitations. It is found that surface plasmon excitations make significant contributions to the XPS in single and plural energy-loss peaks and in the multiple loss background. The computed XPS including surface excitations agrees quite well with experimental data.

2. Interaction cross sections

Elastic and inelastic interactions of electrons in solids contribute mainly to, respectively, the angular deflection and the energy loss of these electrons [18]. Inelastic interactions include excitations of the valence band and of inner shells. For electron energies involved in Au 4f XPS, valence band excitations dominate the energy losses of electrons. Electrons in the solid in the deep region (volume excitations) as well as in the shallow region (surface excitations) contribute to these excitations. In the case of volume excitations, both interband transitions (single-particle excitations) and bulk plasmon oscillations (collective oscillations) are possible. For surface excitations, surface plasmons are generated by the surface charge density fluctuations.

2.1. Elastic scatterings

Since we deal with the transport of Au 4f photoelectrons in Au, electron energies are below ~1410 eV. These energies are less than the Born threshold [19], i.e. $E < 15Z^2$ eV, where Z is the atomic number, so that the Born approximation is poor in the description of elastic scatterings. Here, we apply the partial-wave expansion method to evaluate the differential elastic cross section according to [13]

$$\frac{d\sigma}{d\Omega} = \frac{1}{8E}\left|\sum_{l=0}^{\infty}(2l+1)(e^{2i\delta_l}-1)P_l(\cos\theta)\right|^2, \qquad (1)$$

where $d\Omega = 2\pi(\sin\theta)d\theta$, θ is the scattering angle, E is the electron kinetic energy, k is the momentum transfer, δ_l is the lth phase shift, and $P_l(\cos\theta)$ is the Legendre polynomial of order l. Note that all quantities and expressions in this paper are in atomic units unless otherwise specified. The lth phase shift may be given in the WKB method [20,21] as

$$\delta_l(k) = \frac{(l+1/2)\pi}{2} - kr_0 + \int_{r_0}^{\infty} dr\left\{\left[k^2 - U_{\rm eff}(r)\right]^{1/2} - k\right\}, \qquad (2)$$

where

$$U_{\rm eff}(r) = \frac{l(l+1)}{r^2} + 2V(r) + \frac{1}{4r^2} \qquad (3)$$

is the effective scattering potential for the lth phase shift, $V(r)$ is the elastic scattering potential, and r_0 is the larger root of the equation $k^2 - U_{\rm eff}(r) = 0$. The scattering potential for a solid atom may be determined by

$$V(r) = -\frac{Z}{r} + \frac{1}{r}\int_0^r 4\pi r'^2 n(r')dr' + \int_r^{R_{\rm WS}} 4\pi r' n(r')dr', \qquad (4)$$

where $R_{\rm WS}$ is the Wigner–Seitz radius and $n(r)$ is the HFWS electron density distribution of the solid atom [22].

One may calculate the elastic electron MFP, λ_e, according to

$$\frac{1}{\lambda_e} = N\int \frac{d\sigma}{d\Omega}d\Omega, \qquad (5)$$

where N is the atomic density of the solid. For a measure of the effectiveness of elastic scatterings in causing deflection of the electrons, one may also calculate the electron transport mean free path using [23]

$$\frac{1}{\lambda_t} = N\int(1-\cos\theta)\frac{d\sigma}{d\Omega}d\Omega. \qquad (6)$$

A large difference between λ_e and λ_t indicates that elastic scatterings are predominantly in the forward direction.

2.2. Volume excitations

For inelastic interactions of the photoelectrons with the solid, the response of the solid may be characterized by a dielectric function [24]. In the deep region of the solid, the electron DIMFP for volume excitations is given by [25]

$$\mu_v(E,\omega) = \frac{1}{\pi E}\int_{k_-}^{k_+}\frac{1}{k}{\rm Im}\left[\frac{-1}{\epsilon(k,\omega)}\right]dk, \qquad (7)$$

where ω is the energy transfer, $k_\pm = \sqrt{2E} \pm \sqrt{2(E-\omega)}$ are derived from conservations of energy and momentum, and ${\rm Im}(-1/\epsilon)$, the negative inverse dielectric function, is the bulk energy-loss function. Eq. (7) is valid for $E > 7E_F$ [26,27], where E_F is the Fermi energy of the valence band. Since $E_F \approx 25$ eV for Au, this equation works quite well for Au 4f photoelectrons in Au.

In the deep region of the solid, the electron inverse mean free path (IMFP) for volume excitations can be calculated from

$$\mu_v(E) = \lambda_v^{-1}(E) = \int_0^E \mu_v(E,\omega)d\omega. \qquad (8)$$

In the shallow region, the electron IMFP is modified by a reduction in the volume excitations and by an addition due to surface excitations. This IMFP for volume excitations at a depth z below the surface is approximately given by

$$\mu_v(E,z) = (1-e^{-\omega_p z/v})\mu_v(E), \qquad (9)$$

where ω_p is the free-electron plasma energy. Note that $u_v(E,z)$ vanishes at $z=0$ due to the orthogonality of bulk and surface plasmons [16]. This function approaches the asymptotic value in the deep region, i.e. $\mu_v(E)$ in Eq. (8), as $z \gg v/\omega_p$. The spatially-varying electron IMFP given in Eq. (9) makes MC simulations difficult in the shallow region. The application of Poisson stochastic processes, however, eliminates these difficulties by applying the total probability for inelastic interactions rather than the probability per unit pathlength. The total probability for volume excitations by an electron traveling a distance $D\sec\alpha$ in the shallow region is determined by

$$P_v(E) = \sec\alpha \int_0^D \mu_v(E,z)\,dz, \tag{10}$$

where D is the depth of the shallow region and α is the exit angle relative to the surface normal. Substituting Eq. (9) into Eq. (10), we find

$$P_v(E) = \sec\alpha \left[D - \frac{v}{\omega_p}\left(1 - e^{-\omega_p D/v}\right)\right]\mu_v(E). \tag{11}$$

2.3. Surface excitations

The electron IMFP for surface excitations as a function of depth has been derived using a simple-metal model [16]. It was shown that this quantity has a maximum at the surface and drops off to zero at a distance on the order of angstroms on both sides of the surface. Such a spatially-varying surface plasmon IMFP suggests also that Poisson processes should be applied in the shallow region. Previously [13], we have worked out the differential probability for surface excitations for obliquely incident electrons considering the recoil effect. For fast electrons, this effect was usually neglected by replacing $k^2/2 - \boldsymbol{k}\cdot\boldsymbol{v}$ by $-\boldsymbol{k}\cdot\boldsymbol{v}$ [28]. In our previous work, we added a reduction term in the probability for volume excitations in order to explore the surface-specific effect. Since the spatially-varying electron IMFP in Eq. (9) already contains such a term, we then need to modify the formulas given in Ref. [13] to find the differential probability for surface excitations. This modification may be made by replacing $\mathrm{Im}[(\epsilon-1)^2/\epsilon(\epsilon+1)]$ by $\mathrm{Im}[-4/(\epsilon+1)]$. It can be demonstrated by writing $\mathrm{Im}[(\epsilon-1)^2/\epsilon(\epsilon+1)] = \mathrm{Im}[-4/(\epsilon+1)] - \mathrm{Im}(-1/\epsilon)$, where $\mathrm{Im}[-4/(\epsilon+1)]$ and $\mathrm{Im}(-1/\epsilon)$ have maxima at, respectively, the surface and bulk plasmon energies.

The probability per unit energy-loss for an electron of energy E to lose energy ω in surface excitations is given by

$$P_s(E,\omega) = P_{s+}(E,\omega) + P_{s-}(E,\omega). \tag{12}$$

The positive (negative) index denotes the like (opposite) sign between the scattering angle, θ, and the exit angle, α. Explicitly, we can write

$$P_{s\pm}(E,\omega) = \frac{2}{\pi v^2 \cos\alpha}\int_{k_-}^{k_+}\frac{|k_s'|}{k^3}\,\mathrm{Im}\left[\frac{-4}{(\epsilon+1)}\right]dk, \tag{13}$$

where

$$k_s' = \left[k^2 - \left(\frac{\omega}{v} + \frac{k^2}{2v}\right)^2\right]^{1/2}\cos\alpha \pm \left(\frac{\omega}{v} + \frac{k^2}{2v}\right)\sin\alpha. \tag{14}$$

The positive and negative indices in Eq. (13) indicate an asymmetric effect in the surface excitation probability due to different scattering-angle orientations. This effect has been confirmed experimentally [29]. The total probability for surface excitations by an electron crossing a surface or interface may be obtained from

$$P_s(E) = \int_0^E P_s(E,\omega)\,d\omega. \tag{15}$$

2.4. Dielectric functions

Calculations of electron inelastic cross sections for volume and surface excitations require the dielectric function of the solid. For a free-electron-like material, this function may be characterized by the Drude model [30]. This model, however, is poor in the description of the energy-loss function, exhibiting interband transition peaks with broad and overlapping features. In the case of Au, for instance, modifications must be made to the model to allow individual oscillator strengths, damping coefficients, and critical-point energies for each excitation. The real and imaginary parts of the dielectric function at zero momentum transfer, i.e. the optical limit, are given in the modified Drude model as [16,31]

$$\epsilon_1(0,\omega) = \epsilon_b - \sum_{i=v}\frac{A_i\left[\omega^2 - \omega_i^2\right]}{\left[\omega^2-\omega_i^2\right]^2 + \omega^2\gamma_i^2} \tag{16}$$

and

$$\epsilon_2(0,\omega) = \sum_{i=v}\frac{A_i\gamma_i\omega}{\left[\omega^2-\omega_i^2\right]^2 + \omega^2\gamma_i^2}, \tag{17}$$

where ϵ_b is the background dielectric constant accounting for the effect of polarizable ion cores and A_i, γ_i and ω_i are, respectively, the oscillator strength, damping coefficient, and critical-point energy associated with the ith excitation. Summations in Eqs. (16) and (17) run over all valence electron excitations (denoted by the index v). Thus, it is required that $\sum_i A_i = 4\pi n_v$, where n_v is the number of valence electrons per unit volume.

The above optical dielectric function may be generalized to the region of $k>0$ by replacing ω_i in Eqs. (16) and (17) by $\omega_i + k^2/2$ [25]. This generalization utilizes the asymptotic behavior of the dielectric function at the two ends of k, i.e. the optical limit $k\to 0$ and the Bethe ridge limit $k\to\infty$. All parameters in the modified Drude dielectric function, i.e. ϵ_b, A_i, γ_i and ω_i, can be determined by a fit of Eq. (17) to experimentally measured optical data.

To ensure that fitting results are accurate, we apply two sum rules to check the validity of the model dielectric function. These sum rules are

$$\int_0^\infty \omega\epsilon_2(0,\omega)\mathrm{d}\omega = \frac{\pi}{2}\sum_i A_i = \frac{\pi}{2}\omega_p^2 \tag{18}$$

and

$$\int_0^\infty \omega\,\mathrm{Im}\left[\frac{-1}{\epsilon(0,\omega)}\right]\mathrm{d}\omega = \frac{\pi\omega_p^2}{2\epsilon_b^2}. \tag{19}$$

3. Electron transport

As sketched in Fig. 1, a photoelectron (triangle) ejected by an X-ray photon travels zigzag paths in the solid due to elastic (squares) and inelastic (circles) interactions. Electrons of the solid near the surface are responsible for surface excitations (solid circles), whereas those residing deep inside contribute to volume excitations (open circles). The assumptions that elastic and inelastic interactions contribute to, respectively, angular deflection and energy loss are valid from the following standpoints. First, the ratio of elastic energy loss to inelastic energy loss is on the order of m_e/m_A, where the electron mass, m_e, is much smaller than the nuclear mass, m_A. Second, the scattering angle in inelastic interactions is on the order of ω/E, which is quite small for electron energies considered in this work.

To deal with the transport of photoelectrons in the solid, we apply MC simulations in the deep region and Poisson stochastic processes in the shallow region. These simulations begin with the ejection of photoelectrons by incident X-rays. The photoelectrons are assumed to be randomly produced along the paths of incident photons. The angular distribution of these electrons is determined by the differential photoionization cross section. This cross section for the ionization of an nl-subshell by unpolarized X-rays is given by [32,33]

$$\frac{\mathrm{d}\sigma_{nl}}{\mathrm{d}\Omega} = \frac{1}{4\pi}\left[1+\frac{\beta}{2}\left(\frac{3}{2}\sin^2\phi - 1\right)\right], \tag{20}$$

where $\Omega = 2\pi\sin\phi\,\mathrm{d}\phi$, ϕ is the angle between the incident photons and the emitted photoelectrons, and β is the asymmetry parameter. In this work, we take $\beta = 1.03$ for Au 4f photoelectrons ejected by Al Kα X-rays [33]. The energy distribution of photoelectrons that have not been inelastically scattered is assumed to obey the Lorentzian–Gaussian mixed function [34]

$$f(E) = \frac{\text{peakheight}}{\left[1+M(\Delta E/\gamma)^2\right]\exp\left\{(1-M)\ln\left[2(\Delta E)^2/\gamma^2\right]\right\}}. \tag{21}$$

where $E = E_0 - \Delta E$, E_0 is the peak energy, γ is related to the full width at half maximum of this distribution, and M is the Lorentzian–Gaussian mixing ratio. Values adopted in this work are $\gamma = 0.46$ eV and $M = 0.89$. Eq. (21) is a reasonable approximation to experimentally measured photoelectron lineshapes.

In the deep region, electrons may interact with the solid through elastic scatterings and inelastic volume excitations. The actual type of interaction, the angular deflection, and the energy loss are determined in MC simulations through the relevant differential cross sections and random number generations. These simulations proceed until all electrons either enter the shallow region or their energies fall below a specified value. In the shallow region, electrons may interact with the solid through additional surface excitations. Since electron DIMFPs for both volume and surface excitations become spatially-varying in this region, MC simulations tend not to be feasible. This situation arises because it is not practical to sample a wide range of inelastic cross sections covering all depths due to the low yield of photoelectrons and the small thickness of the shallow region. The fact that surface plasmons may be excited by emerging electrons in the vacuum further complicates these simulations. The application of Poisson processes, however, is useful since integrated cross sections over all depths are employed. This application is valid in the shallow region because it extends into the solid only a few angstroms, on the order of one inelastic MFP. Thus, electron inelastic MFP in the shallow region may be assumed to be a constant everywhere inside this region.

The excitation of n surface plasmons by an electron of energy E crossing a solid–vacuum interface obeys the Poisson distribution

$$F_s^{(n)} = \frac{P_s(E)^n e^{-P_s(E)}}{n!}, \tag{22}$$

where $P_s(E)$ is given in Eq. (15). Similarly, the excitation of n bulk plasmons in the shallow region is given by

$$F_v^{(n)} = \frac{P_v(E)^n e^{-P_v(E)}}{n!}, \tag{23}$$

where $P_v(E)$ is given in Eq. (11). With $F_s^{(n)}$ and $F_v^{(n)}$ determined, one can estimate the energy loss of an electron passing through the shallow region using the differential probability functions of Eqs. (12) and (7).

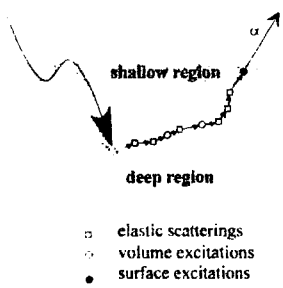

Fig. 1. A sketch of the zigzag trajectory of a photoelectron ejected by an X-ray inside the solid for XPS simulations. Here, α is the emission angle.

For photoelectrons ejected from the shallow region, the above probabilities, $P_s(E)$ and $P_v(E)$, must be modified. In the case of volume excitations, the upper limit of integration in Eq. (10) should be replaced by the depth at which photoelectrons are produced. For surface excitations, a similar replacement should be made.

4. Results and discussion

Using the partial-wave expansion method with the WKB approximation, we have calculated electron differential elastic cross sections in Au. Fig. 2 shows some representative results of these calculations as a function of scattering angle, θ, for electrons of several energies. It is seen that elastic scatterings are predominantly in the forward direction with enhanced small-angle scatterings for high-energy electrons. Fig. 2 also reveals that the elastic cross sections decrease smoothly with increasing θ for $\theta < 20°$, but fluctuate for $\theta > 20°$. This fluctuation, owing to the screening of nuclear charge by atomic electrons in different shells, becomes larger for lower energy electrons due to the longer scattering time. In Fig. 3 we plot electron MFPs in Au for elastic scattering, λ_e, for transport scattering, λ_t, and for volume excitations, λ_v, as a function of electron energy. Fig. 3 shows that for most electron energies λ_e is smaller than λ_v by a factor of no more than 2. In other words, each volume excitation in Au is accompanied by one to two elastic scatterings. The significant difference between λ_e and λ_t indicates that elastic scattering is predominantly in the forward direction. For comparison, we also plot in this figure results from other calculations. The solid circles [35] are electron inelastic MFPs calculated using experimental optical data and the theoretical Lindhard dielectric function. The solid and open triangles [36] are, respectively, electron transport and elastic MFPs

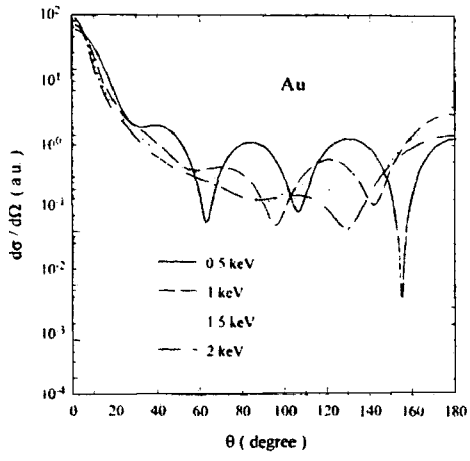

Fig. 2. A plot of the differential elastic cross section as a function of scattering angle for electrons of several energies in Au. This cross section is expressed in atomic units.

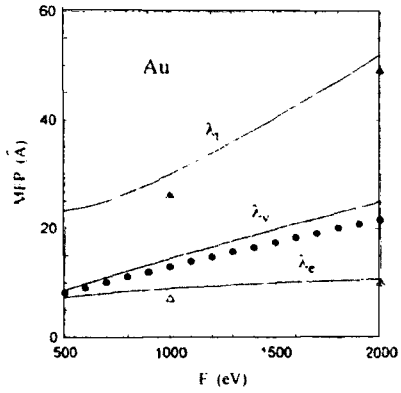

Fig. 3. A plot of electron mean free path for elastic scattering, λ_e, transport scattering, λ_t, and volume excitations, λ_v, as a function of electron energy in Au. The solid circles are electron inelastic MFPs from other calculations [35]. The solid and open triangles are, respectively, electron transport and elastic MFPs from other calculations [36].

calculated using the static approximation with Hartree–Fock atomic wavefunctions. The minor differences between the present and other calculated results reflects deviations due to different models.

Table 1 lists parameters in the model dielectric function of Eqs. (16) and (17) for Au determined from fits to the data of Ref. [30]. In these fits, we check not only the accuracy of $\epsilon_1(0,\omega)$, $\epsilon_2(0,\omega)$ and $\mathrm{Im}[-1/\epsilon(0,\omega)]$ obtained from the present calculations, but also the extent to which they satisfy the sum rules. Note that the upper limit of integration in Eqs. (18) and (19) is infinity. If we set this limit to a finite value, the contribution from valence electrons is not exhausted. On the other hand, inner-shell contribution may occur before the exhaustion of valence electrons. For a useful check on the derived dielectric function, we fit Eq. (17) to experimental data for energy losses which cover the loosely bound 5s and 5p subshells. Because of the overlap of oscillator strengths between the

Table 1
Parameters in the model dielectric function of Eqs. (16) and (17) for Au; $\epsilon_b = 1.01$

A_i [eV^2]	γ_i [eV]	ω_i [eV]
79	0.1	0.0
9	1.0	3.1
36	1.9	4.1
17	2.3	5.3
60	4.0	8.17
100	9.0	12.0
120	10.0	14.0
155	6.0	21.3
145	7.2	29.5
280	20.0	38.5
360	28.0	63.0
183	26.0	100.0

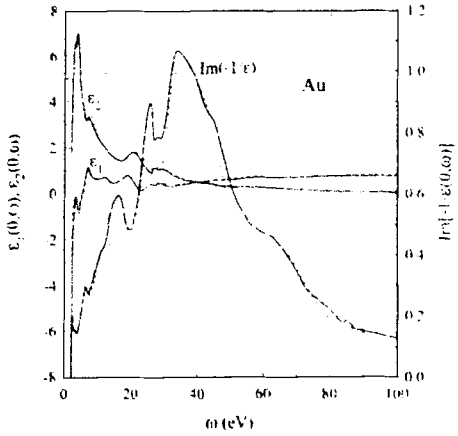

Fig. 4. A comparison of experimental data (solid curves) [30] and calculated results (dashed curves) for the real part of the dielectric function, ϵ_1, the imaginary part, ϵ_2, and the energy-loss function, $\mathrm{Im}(-1/\epsilon)$, in the optical limit, i.e. $k \to 0$, for Au.

valence band and these subshells, we require that the saturation number of electrons contributing to energy losses up to ~ 100 eV equals 19. This is reasonable since the overlap of oscillator strengths between the valence band and other inner shells is negligibly small. The influence of inner shell electrons on the dielectric function is contained in the background dielectric constant appearing in Eq. (16). A detailed discussion about this constant is given elsewhere [31]. Fig. 4 shows a comparison of $\epsilon_1(0,\omega)$, $\epsilon_2(0,\omega)$ and $\mathrm{Im}[-1/\epsilon(0,\omega)]$ for Au calculated presently (dashed curves) and measured experimentally (solid curves) [30]. Good agreement is found between the present results and experimental data for all functions plotted.

Based on the model dielectric function, we have calculated electron DIMFPs for volume excitations in an infinite medium of Au. Fig. 5 shows the results of such calculations for electrons of several energies. It is noted that the

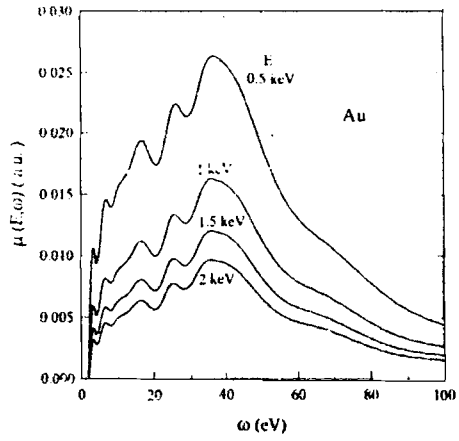

Fig. 5. A plot of the volume excitation DIMFP for electrons of several energies traversing in the deep region of Au. This DIMFP is expressed in atomic units.

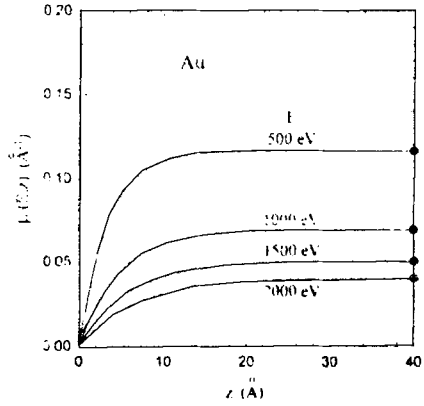

Fig. 6. A plot of electron IMFP for volume excitations as a function of depth in Au for electrons of several energies. Asymptotic values at an infinite depth are depicted as solid circles at 40 Å.

bulk plasmon loss-peak occurs at ~ 37 eV, corresponding to the main peak energy in the energy-loss function of Fig. 4. Fig. 6 shows a plot of electron IMFPs for volume excitations as a function of depth in Au for electrons of several energies. It is seen that the electron IMFP becomes spatially-varying in the shallow region, rising from zero at the surface to a constant value at ~ 10–20 Å. Also depicted in this figure (solid circles at 40 Å) are the spatially non-varying electron IMFPs in an infinite medium of Au. This feature of the depth dependence in the electron IMFP for volume excitations is compensated by the excitation of surface plasmons. The IMFP for surface excitations has a maximum at the surface, and falls off to zero on either side of the surface. Here, we have calculated electron differential probabilities for surface excitations using the same model dielectric function. Fig. 7 shows the results of these calculations for electrons passing through a Au surface with an exit angle of 0°. Two surface plasmon peaks at 3.1 and 5.3 eV are prominent.

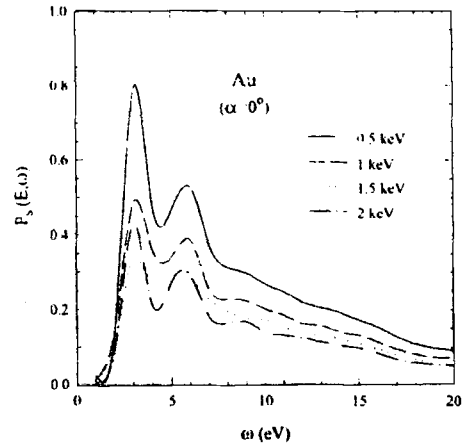

Fig. 7. A plot of the surface excitation differential probability for electrons of several energies crossing the Au–vacuum interface.

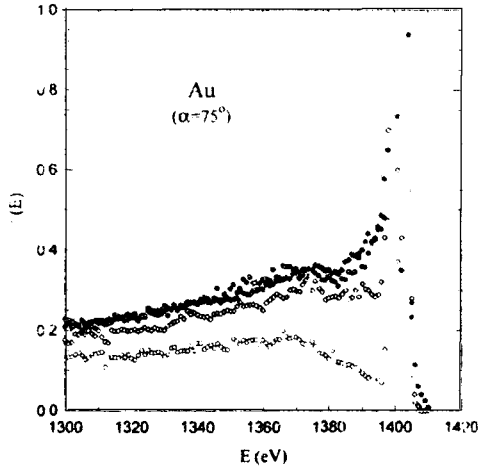

Fig. 8. A comparison of Au 4f XPS at an exit angle of 75° from experimental measurements (solid diamonds) [11], theoretical computations by Yoshikawa et al. (open diamonds) [11] and the present calculations considering (solid circles) and neglecting (open circles) surface excitations.

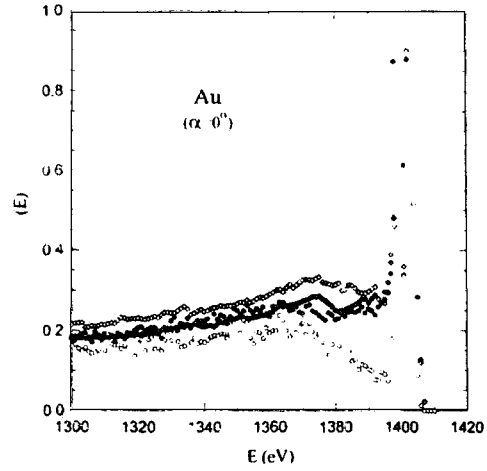

Fig. 9. A comparison of Au 4f XPS at an exit angle of 0° from experimental measurements (solid diamonds) [11], theoretical computations by Yoshikawa et al. (open diamonds) [11] and the present calculations considering (solid circles) and neglecting (open circles) surface excitations.

The generation of Au 4f photoelectrons along the paths of incident Al Kα X-rays is traced to a depth of 100 Å. For photoelectrons generated in the deep region, MC simulations are applied to determine electron trajectories from differential cross sections for elastic scattering and volume excitations. When these electrons enter the shallow region, Poisson processes are used to determine electron trajectories with respect to volume and surface excitations. In the case of photoelectrons produced in the shallow region, Poisson processes are adopted for the determination of electron trajectories. The computer program terminates when all electrons either leave the solid or their energies fall below a cutoff energy of 1300 eV. Electrons escaping from the solid are then registered if they enter the acceptance solid angle of the analyzer. This solid angle corresponds to an acceptance angle within $\pm 4°$ from the central axis of the analyzer. Fig. 8 shows a comparison of experimental data (solid diamonds) [11], present calculations with (solid circles) and without (open circles) surface excitations, and other theoretical results (open diamonds) [10,11] for Au 4f XPS with an emission angle of 75°. In order to compare theoretical results with experimental data on the same basis, all spectra are normalized at the energy of the Au $4f_{7/2}$ photoelectron peak at around 1402.6 eV with a peak height of 5. It is seen that surface excitations make significant contributions to XPS in single and plural energy-loss peaks and to the multiple loss background. The single and plural surface plasmon loss-peaks are easily identified.

A similar comparison for Au 4f XPS is made in Fig. 9 for an exit angle of 0°. Here the contribution from surface excitations to XPS is less pronounced than that for an exit angle of 75°. This is because glancing-emergence electrons travel a longer pathlength in the shallow region than those emitted normally. Hence, the influence of surface excitations is enhanced for larger emission angles, owing to the increased probability for surface excitations. Finally, we compare in Fig. 10 Au 4f XPS for an exit angle of 45°. Again, the contribution from surface excitations to XPS is significant. In all cases, the present results that include surface excitations agree quite well with experimental data. Note that the effective loss-function in the Yoshikawa et al. [10] calculations is extracted from experimental XPS at an exit angle of 45°. Thus, the calculated results by Yoshikawa et al. agree better with experimental data at this emission angle than at other angles. The present XPS

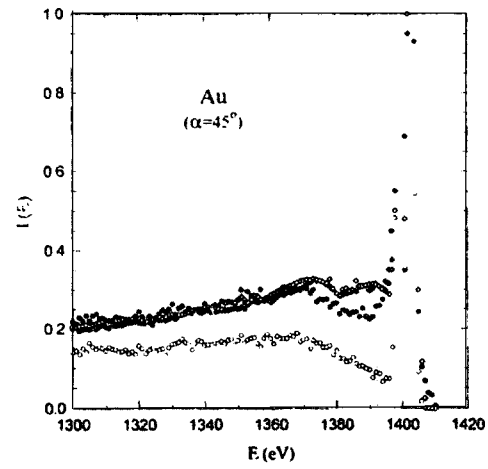

Fig. 10. A comparison of Au 4f XPS at an exit angle of 45° from experimental measurements (solid diamonds) [11], theoretical computations by Yoshikawa et al. (open diamonds) [10,11] and the present calculations considering (solid circles) and neglecting (open circles) surface excitations.

calculations are obtained from theoretical cross sections derived from first principles rather than from a single set of experimental data.

5. Conclusions

Studies have been made to determine the influence of surface excitations on Au 4f X-ray photoelectron spectra. Our approach involved Monte Carlo simulations of photoelectrons in the interior of the solid and Poisson stochastic processes near the surface. Differential cross sections for elastic and inelastic interactions of electrons in Au were determined from model calculations. Electron inverse mean free paths for volume and surface excitations in the surface region were constructed as a function of depth. Computed results on Au 4f XPS showed that surface plasmon excitations made significant contributions to the spectra in single and plural energy-loss peaks and in the multiple loss background. The spectra that included surface excitations agreed quite well with experimental data for different emission angles.

Reference:

[1] C.J. Powell, Surf. Sci. 299/300 (1994) 34.
[2] R.F. Egerton, Electron Energy-Loss Spectroscopy in the Electron Microscope (Plenum, New York, 1986).
[3] C.S. Fadley, R.J. Baird, W. Siekhaus, T. Novakov and S.A.L. Bergstrom, J. Electron Spectrosc. Phenom. 4 (1974) 93.
[4] M.F. Ebel, H. Ebel and K. Hirokawa, Spectrochim. Acta 37B (1982) 461.
[5] A. Jablonski and C.J. Powell, Surf. Interface Anal. 20 (1993) 771.
[6] A. Jablonski, J. Gryko, J. Kraaer and S. Tougaard, Phys. Rev. B 39 (1989) 61.
[7] A. Jablonski, Phys. Rev. B 43 (1991) 7546.
[8] A. Jablonski, H.S. Hansen, C. Jansson and S. Tougaard, Phys. Rev. B 45 (1992) 3694.
[9] A. Jablonski, C. Jansson and S. Tougaard, Phys. Rev. B 47 (1993) 7420.
[10] H. Yoshikawa, R. Shimizu and Z.J. Ding, Surf. Sci. 261 (1991) 403.
[11] H. Yoshikawa, T. Tsukamoto, R. Shimizu and V. Crist, Surf. Interface Anal. 18 (1992) 757.
[12] C.J. Tung, Y.F. Chen, C.M. Kwei and T.L. Chou, Phys. Rev. B 49 (1994) 16684.
[13] Y.F. Chen, C.M. Kwei and C.J. Tung, Phys. Rev. B 50 (1994) 17547.
[14] S. Tougaard and J. Kraaer, Phys. Rev. B 43 (1991) 1651.
[15] F. Yubero and S. Tougaard, Phys. Rev. B 46 (1992) 2486.
[16] P.J. Feibelman, Surf. Sci. 36 (1973) 558.
[17] C.M. Kwei, Y.F. Chen, C.J. Tung and J.P. Wang, Surf. Sci. 293 (1993) 202.
[18] Y.F. Chen, C.M. Kwei and C.J. Tung, J. Phys. D 25 (1992) 262.
[19] H.A. Bethe and R.W. Jackiw, Intermediate Quantum Mechanics, 3rd ed. (Benjamin Cummings, Menlo Park, CA, 1986).
[20] C.J. Jochain, Quantum Collision Theory (North-Holland, Amsterdam, 1975).
[21] F. Salvat, R. Mayol, E. Molins and J. Parallada, J. Phys. D 17 (1985) 185.
[22] T.C. Tucker, L.D. Roberts, C.W. Nestor and T.A. Carson, Phys. Rev. 178 (1969) 998.
[23] A.L. Tofterup, Phys. Rev. B 32 (1985) 2808.
[24] H. Raether, Excitations of Plasmons and Interband Transitions by Electrons, vol. 88 of Springer Tracts in Modern Physics (Springer, New York, 1980).
[25] R.H. Ritchie, R.N. Hamm, J.E. Turner, H.A. Wright and W.E. Bolch, in: Physical and Chemical Mechanisms in Molecular Radiation Biology, eds. W.A. Glass and M.N. Varma (Plenum, New York, 1991).
[26] R.H. Ritchie, C.J. Tung, V.E. Anderson and J.C. Ashley, Radiat. Res. 64 (1975) 181.
[27] M. De Crescenzi, L. Lozzi, P. Picozzi and S. Santucci, Phys. Rev. B 39 (1989) 8409.
[28] P.M. Echenique, F. Flores and R.H. Ritchie, in: Solid State Physics – Advance in Research and Applications, eds. H. Ehrenreich and D. Turnbull (Academic Press, New York, 1990).
[29] R.B. Pettit, J. Silcox and R. Vincent, Phys. Rev. B 11 (1975) 3116.
[30] J. Daniels, C.V. Festenberg, H. Raether and K. Zeppenfeld, Optical Constants of Solids by Electron Spectroscopy, vol. 54 of Springer Tracts in Modern Physics (Springer, New York, 1980).
[31] Y.F. Chen, C.M. Kwei and C.J. Tung, Phys. Rev. B 48 (1993) 4373.
[32] A. Spalek, Surf. Interface Anal. 15 (1990) 739.
[33] R.F. Reilman, A. Msezane and S.T. Manson, J. Electron Spectrosc. Relat. Phenom. 8 (1976) 389.
[34] D. Briggs and M.P. Seah, Practical Surface Analysis by Auger and X-ray Photoelectron Spectroscopy (Wiley, New York, 1984).
[35] S. Tanuma, C.J. Powell and D.R. Penn, Surf. Interface Anal. 17 (1991) 911.
[36] M.E. Riley, C.J. MacCallum and F. Biggs, At. Data Nucl. Data Tables 15 (1975) 443.